

# **Nanoscale friction of manganite superlattice films controlled by layer thickness and fluorine content**

N.A. Weber<sup>1</sup>, M. Lee<sup>2</sup>, F. Schönewald<sup>1</sup>, L. Schüler<sup>3</sup>, V. Moshnyaga<sup>3</sup>, M. Krüger<sup>2</sup> and C.A. Volkert<sup>1,4,5</sup>

<sup>1</sup>Institute of Materials Physics, University of Göttingen, Friedrich-Hund-Platz 1, Göttingen 37077, Germany

<sup>2</sup>Institute for Theoretical Physics, University of Göttingen, Friedrich-Hund-Platz 1, 37077 Göttingen, Germany

<sup>3</sup>1st Physics Institute, University of Göttingen, Friedrich-Hund-Platz 1, 37077 Göttingen, Germany

<sup>4</sup>The International Center for Advanced Studies of Energy Conversion (ICASEC), University of Göttingen, Göttingen 37077, Germany

<sup>5</sup>International Institute for Carbon Neutral Energy Research (WPI-I2CNER), Kyushu University, 744 Motoooka, Nishi-ku, Fukuoka 819-0935, Japan

**Keywords:** atomic force microscopy, lateral force microscopy, friction, superlattices, manganite, internal friction

## Abstract

We investigate nanoscale friction in  $[\text{LaMnO}_3]_m/[\text{SrMnO}_3]_n$  superlattice films using lateral force microscopy, focusing on the effects of fluorine doping and top-layer thickness. For all samples, friction forces scale linearly with the sum of the applied normal and adhesion forces. While friction forces vary spatially due to local adhesion fluctuations, the friction coefficient remains position independent for each specimen. It is, however, systematically influenced by fluorine concentration and top-layer thickness. Our data indicates that frictional energy dissipation extends up to  $\sim 5$  nm beneath the surface, demonstrating a clear dependence on subsurface structure. We attribute this to viscoelastic dissipation within the stress field and evanescent waves generated by the sliding tip, which can quantitatively account for the observed friction coefficients. These results show that, once adhesion is properly accounted for, the friction coefficient is a reproducible material property that can be tuned via controlled modifications to surface and subsurface layers.

## Highlights

1. Nanoscale friction in manganite superlattices is systematically tuned by fluorine doping and top-layer thickness.
2. Frictional energy dissipation extends up to  $\sim 5$  nm below the surface, revealing a key role of subsurface viscoelastic mechanisms.
3. Once adhesion is accounted for, the friction coefficient is a reproducible property that reflects subsurface structure.

## 1. Introduction

Controlling friction at a sliding contact has been a long-standing challenge in technology and society. A large fraction of the energy that society consumes is lost in frictional dissipation,<sup>1</sup> but at the same time, friction is essential to traction and mechanical control. Ideally, ways will be found to turn friction off when it is not needed and to turn it on when forces need to be imparted on the object. A significant amount of research has focused on trying to control friction, and with the emergence of atomic force microscopy (AFM) in the 1980s,<sup>2</sup> friction at a nanoscale contact could be studied, allowing insights into fundamental mechanisms of energy loss.

A general picture for dry, low wear friction has emerged out of these studies. Most importantly, the ground-breaking work of Bowden and Tabor showed that a mesoscopic contact consists of numerous, individual asperity contacts. They argued that the measured friction force is proportional to the true area of contact and not the apparent contact area.<sup>3</sup> Numerous studies have tested this idea, by measuring both the contact area and the friction force; and, many studies support the hypothesis, at least within the typically large measurement scatter.

Not surprisingly then, many discussions of friction between hard materials have focused on dissipation mechanisms occurring directly in the contact interface.<sup>4</sup> However, several recent studies have also shown evidence for possible sub-surface contributions to the friction of hard materials. The reported experimental observations are all based on measuring the change in friction as a result of changing material properties by varying the temperature,<sup>5–8</sup> contact pressure,<sup>9</sup> or bias voltage/carrier density.<sup>10–13</sup> Significant changes in friction have been reported that correlate with changes in phononic and electronic degrees of freedom in the material, and a variety of models have been proposed to attempt to account for these. However, in most cases, the model predictions, which are based on dissipation through phononic and electronic degrees of freedom, are too small to account for the observed effects.<sup>14</sup> Furthermore, all the studies are weakened by the fact that the applied fields change the properties of the specimen surfaces as well as of the sub-surface material, so that it is not clear whether the observed effects are from changes in dissipation in the specimen volume or from changes in dynamics in the sliding contact.

In addition to phononic and electronic degrees of freedom, viscoelastic contributions from sub-surface regions to friction have also been considered, particularly for the case of elastomers such as rubber. As early examples, internal friction or elastic hysteresis losses have been proposed as

the main origin of rolling friction on rubber and several metals<sup>15</sup> and of sliding friction on rubber.<sup>16</sup> Various quantitative models have been proposed for rubber friction and critically compared,<sup>17</sup> that are often based on the idea that friction forces and coefficients are the sum of two terms: a term proportional to the true contact area that scales with adhesion hysteresis and a term proportional to the stressed volume and the internal friction of the material.

An experimental approach that allows volume and surface effects to be more clearly differentiated is to study specimens where the top surface layer remains unchanged, while the materials below are varied. The existing literature on layered materials, such as graphene, provide examples of this, where friction has been observed to decrease with increasing layer count.<sup>18</sup> The observed layer dependence is often attributed to puckering effects, which are only expected in materials with weak interlayer forces. Possible contributions from electron-phonon coupling have also been considered<sup>19</sup> although at least one report claims they are negligible.<sup>20</sup> More relevant to the work here is a theoretical study on friction of a layered material, where friction results from the viscous dissipation within the evanescent waves and stress fields excited below the surface by a vibrating tip.<sup>21</sup>

In the work discussed here, we present AFM sliding friction measurements on six  $[\text{LaMnO}_3]_m/[\text{SrMnO}_3]_n$  superlattice films, with varying layer thicknesses in the range 2 to 20 atomic layers (or 0.8 to 8 nm). The films were found to be doped with fluorine, which strongly affected the measured friction coefficients, complicating the systematic investigation of the effect of layer thickness. However, in several films with similar fluorine content, we find indications that top layer thicknesses below around 3 nm affect friction, suggesting that dissipation occurs in the sub-surface material to a depth of 3 nm. We also find that the friction coefficient is consistently constant for a given film, although the friction forces may vary considerably as a function of position due to effects of adhesive forces, suggesting that there may be the possibility to systematically control sliding friction coefficients at manganite surfaces through their composition and surface layer thickness.

## 2. Experimental Section

### 2.1 Specimen Preparation and Characterization

Epitaxial superlattice films of  $[\text{LaMnO}_3]_m/[\text{SrMnO}_3]_n$ , where  $m$  refers to the number of  $\text{LaMnO}_3$  unit cell layers, and  $n$  to the number of  $\text{SrMnO}_3$  unit cell layers, were grown using metal organic

aerosol deposition technique (MAD).<sup>22</sup> An overview of the m to n ratio of the films studied here can be found in **Table 1**. Each superlattice stack was terminated with a layer of  $[\text{LaMnO}_3]_m$  to ensure equivalent chemical composition on the surface. The layer thicknesses and periodicities were monitored during deposition using in-situ ellipsometry measurements. The total superlattice film thicknesses were kept constant at around 31 nm. All films were deposited on  $5 \times 5 \times 0.5 \text{ mm}^3$  (100)-oriented  $\text{SrTiO}_3$ : 1.0 at. % Nb  $K \leq 0.5^\circ$  substrates.

The films were characterized after deposition using standard x-ray methods.  $\theta - 2\theta$  diffraction (XRD) confirmed heteroepitaxy and no reflexes related to impurities. Small-angle x-ray scattering (XRR) provides the superlattice reflections which are used to confirm layer thickness and revealed intensities consistent with an interface roughness of  $\text{RMS} \leq 0.6 \text{ nm}$  for all films. Additionally, the magnetic properties of the films were characterized by temperature dependent measurements of the magnetic moment (SQUID).

The thermal resistivities  $\kappa^{-1}$  of the films studied here were estimated from prior measurements on superlattice films deposited using identical protocols and in the same deposition chamber.<sup>23</sup> Specifically,  $\kappa^{-1}$  values for various  $[\text{LaMnO}_3]_m/[\text{SrMnO}_3]_n$  films, including those with the same m and n ratios as in this study, were obtained via optical transient thermal reflectivity and showed a linear dependence on interface density. This linear relation was used to estimate the  $\kappa^{-1}$  values of the films used here, listed in **Table 1**. The comparison is further supported by SQUID measurements, which confirmed that the magnetic properties of the present films align well with those reported earlier.<sup>23,24</sup>

**Table 1.**  $[\text{LaMnO}_3]_m/[\text{SrMnO}_3]_n$  superlattice film layer thicknesses and thermal resistivities. Individual layer thickness was obtained from XRR measurements. Thermal resistivity values were approximated from thermal transient reflectivity measurements.  $\text{LaMnO}_3$  is either cubic ( $m/n = 1$ ) or rhombohedral ( $m/n = 2$ ), depending on the m/n ratio.

m	n	Film thickness	Thermal resistivity $\kappa^{-1}$
[3.9 Å]	[3.9 Å]	[nm]	[mK/W]
2	2	32	0.91(2)
4	2	34	3.27(7)
6	6	32	0.43(2)
8	4	31	1.84(7)
14	7	32	1.23(7)

XPS measurements were used to determine the chemical composition of the manganite film surfaces. The expected La, Sr, Mn, and O peaks were observed, as were peaks for C and F (**Figure 1**). The compositional ratios of (La+Sr)/Mn and Sr/La were estimated using standard methods and found to fall in expected ranges, within the experimental accuracy. The full spectra, as well as further details on the evaluation, are presented in the supporting information.

Fluorine is known as a source of contamination in materials prepared in systems containing Teflon components.<sup>25</sup> This is probably the source of fluorine in the superlattice films since the MAD deposition chamber contained Teflon parts at the time the films were deposited. If fluorine is present as a contaminant on the sample surface, a F-1s binding energy of 689.8 eV is expected, together with a C-1s signal at 292.5 eV, reflecting C-F bonds.<sup>25</sup> However, the measured F-1s binding energy is significantly smaller at 684.45 eV and no component in the C-1s peaks at 292.5 eV is observed (see **Figure 1a**). Therefore, we can rule out that F is present as a surface contaminant. Instead, the binding energy of the F-1s peak matches with SrF<sub>2</sub> (684.6 eV)<sup>26</sup> or LaF<sub>3</sub> (684.5 eV),<sup>27</sup> suggesting that F replaces oxygen in our films, as has been observed in fluorine doped SrMnO<sub>3</sub>.<sup>28</sup> The fluorine content in our films, was estimated from the F-1s and Mn-2p peak intensities using standard methods (see **Figure 1b**) and found to replace oxygen at a fraction between 0.1 and 0.4. The films with top layer thickness of  $m = 2, 4$  and 14 exhibit a particularly high F concentrations compared to the other four superlattice films.

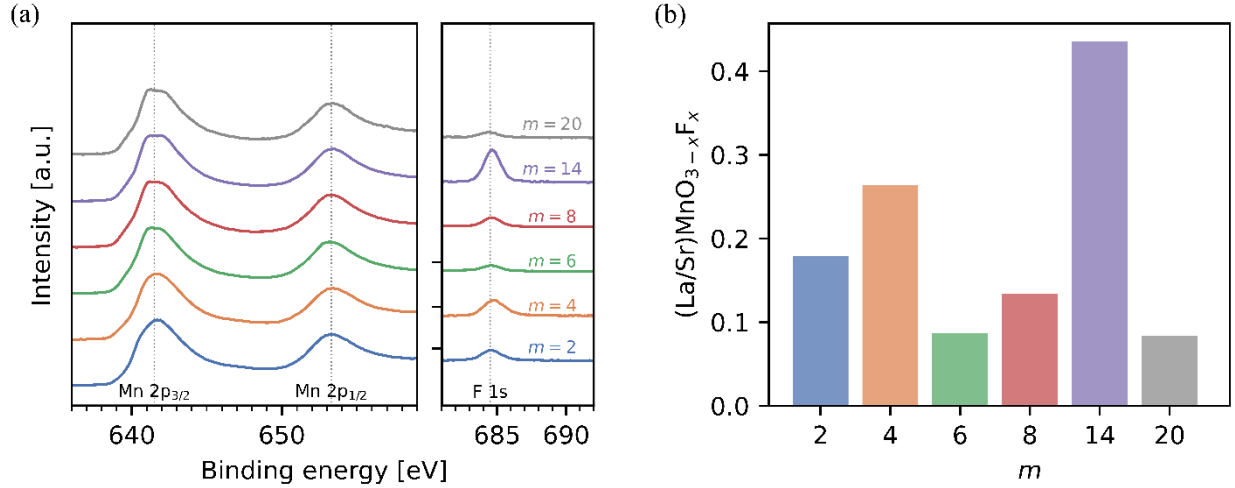


Figure 1: (a) XPS spectra showing the Mn-2p<sub>1/2</sub> and Mn-2p<sub>3/2</sub> peaks at binding energies of 653 eV and 641 eV, and the F-1s peak at a binding energy of 685 eV. (b) The fluorine concentration in the near surface region of the superlattice samples is determined from the ratio of the Mn to F peak areas.

## 2.2 Lateral Force Microscopy

Friction measurements were performed using the lateral force microscopy method in an AFM at room temperature ( $T = 293$  K) under UHV ( $p \approx 2 \times 10^{-10}$  mbar) conditions. The torsion of the cantilever is measured as it is laterally dragged over the film surface at a constant applied normal force  $F_N$  and velocity ( $v = 250$  nm s<sup>-1</sup>) and is directly proportional to the lateral forces  $F_L$  during sliding. To separate changes in topography from friction effects, so-called friction loops – trace and retrace scanning along the same line on the film surface – are recorded, to yield the friction force  $F_F = 1/2 \cdot (F_{L,\text{trace}} - F_{L,\text{retrace}})$ .<sup>29</sup>

Friction forces  $F_F$  were obtained by averaging over 50 friction loops that were recorded within a  $100 \times 250$  nm<sup>2</sup> surface region with a point density of 1 nm<sup>-1</sup> along the fast, and 0.5 nm<sup>-1</sup> along the slow scan direction for each normal load and film. To assess how robust and reproducible the friction measurements are and to determine the order of magnitude of possible variations, the measurements were repeated several times on randomly selected areas on the film surface. In addition, to minimize wear during the friction experiments, the applied normal forces  $F_N$  were kept below 30 nN and any possible changes in the contact were monitored through adhesion measurements.

By measuring the frictional forces on the same surface area as a function of an applied load, a friction coefficient  $\mu$  between the tip and the specimen can be determined using a modified Amontons relation

$$F_F = \mu \cdot F_N + F_{F0}, \quad (1)$$

where the term  $F_{F0}$  is the non-vanishing frictional force at  $F_N = 0$  N. It is non-zero due to adhesion forces  $F_A$  between tip and film, which become comparable to the friction forces at the nanoscale.<sup>29</sup>

Adhesion forces were equated to the pull-off forces obtained by averaging over 50 force-distance curves.<sup>17</sup> Significant changes in adhesion forces before and after probing the frictional properties can indicate changes in tip geometry due to wear, changes in the surface chemistry, or electrostatic forces due to triboelectrification.<sup>30</sup> To confirm that our friction measurements did not alter the surface morphology or affect the friction forces measured, an overview height map and lateral force scan of the measurement area was performed after friction measurements.

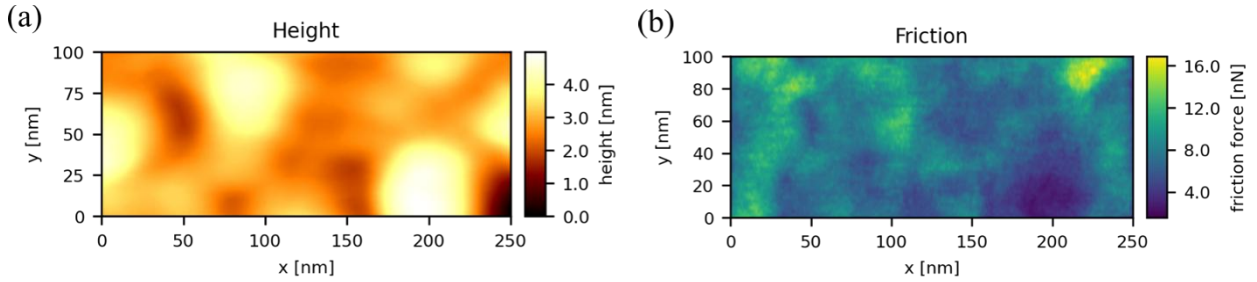


**Figure 2.** (a) Topography and (b) corresponding friction force  $F_F$  maps of a  $[\text{LaMnO}_3]_2/[\text{SrMnO}_3]_2$  surface obtained under a normal load of 28 nN. There is no obvious correlation between the friction force map and the topography.

### 3. Experimental Results

**Figure 2** shows a height map and the corresponding friction force map for a  $[\text{LaMnO}_3]_2/[\text{SrMnO}_3]_2$  film. The height map has an RMS roughness of less than 0.5 nm and a typical feature size of around 50 nm, while the friction force map shows factor of four variations with feature sizes ranging from 50 nm down to around 5 nm. Spearman correlation coefficients of  $r_s = 0.029$  between the friction and height maps and of  $r_s = 0.125$  between the friction and height gradients along the x-direction, rule out correlations between friction and topography and support the validity of the lateral force



method to measure friction.<sup>29</sup> Similar surface topographies and friction maps were obtained on all  $[\text{LaMnO}_3]_m/[\text{SrMnO}_3]_n$  films and show comparably low correlations  $r_S < 0.15$ .

According to Hertz contact theory, the contact area between the nominally 10 nm radius AFM tip and a flat sample surface should have a contact radius between 0.5 and 1.5 nm, for the range of normal forces experienced here. The characteristic topographical feature size in **Figure 2(a)** is around 50 nm, which suggests that the surface is smooth below this length scale. However, roughness within the contact area at length scales of smaller than 0.5 nm, such as due to atomic scale roughness, cannot be ruled out. In fact, atomic scale roughness would lead to multiple asperities within the contact area and can explain the local variations in friction force observed over length scales as small as 10 nm (**Figure 2(b)**).

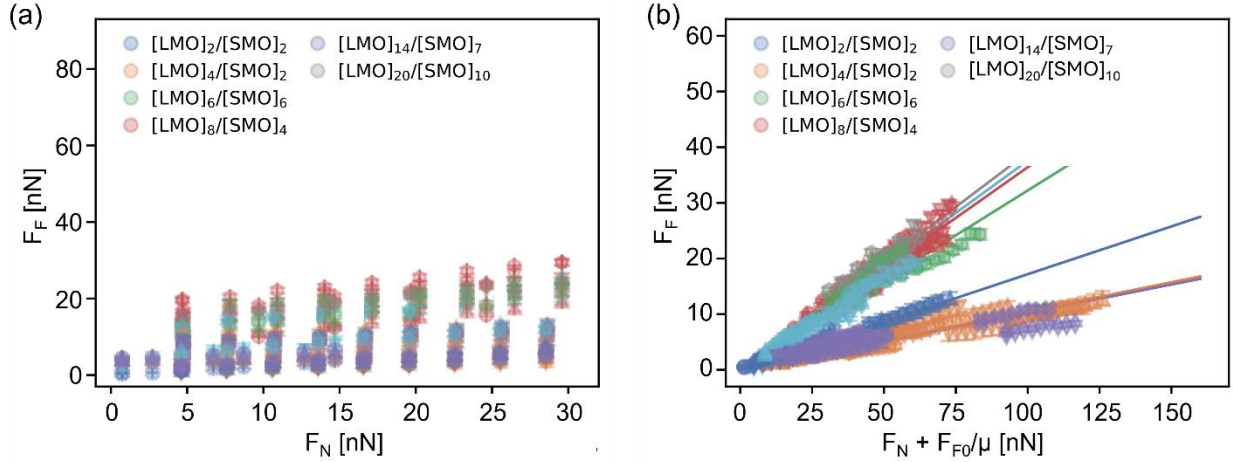


**Figure 3.** Average friction forces  $F_F$  of the  $[\text{LaMnO}_3]_m/[\text{SrMnO}_3]_n$  films plotted as a function of (a) the applied normal load  $F_N$  (Amontons measurement), and (b) the total normal load  $F_N + F_{F0}/\mu$ .

The friction force  $F_F$  for a given film and for a given applied normal load  $F_N$  was obtained by averaging over an individual friction map (250 nm  $\times$  100 nm region). Sets of friction maps obtained for different applied normal loads between 1 and 30 nN were performed within around a micrometer distance of each other on the sample surface and used to obtain so-called Amontons measurements (friction force versus normal force). These Amontons measurements all show linear behavior, and linear regressions were performed to obtain the non-zero friction force intercept  $F_{F0}$  (Equation 1) as well as a friction coefficient  $\mu$  (slope) for each Amontons measurement (**Figure (a)**). Several Amontons measurements were obtained for each sample. While the slopes  $\mu$  did not vary much for a given sample, vertical shifts in data led to wide variations in  $F_{F0}$  with no

clear dependence on nominal layer thicknesses or other material properties. Shifts as large as 10 nN were found between sets of maps performed at randomly selected regions on a given film surface using a single AFM tip. These are likely due to local changes in surface chemistry, carbon-based surface residues, and adsorbed water. And shifts as large as 50 nN occurred between Amontons measurements performed on a given sample using different AFM cantilevers. These are attributed to changes in tip shape and contact area.

The widely shifted Amontons measurements (**Figure 3(a)**) can be transformed into well-behaved proportional dependences of the friction force on the sum of the applied normal load  $F_N$  plus  $F_{F0}/\mu$  (**Figure (b)**). The value  $F_{F0}/\mu$  reflects the (tensile) normal force that must be applied to the tip to overcome adhesion and separate the two surfaces, assuming a linear dependence between friction and normal force.  $F_{F0}/\mu$  is thus expected to correlate with the pull-off forces obtained from force-distance-curves, which also reflect the adhesive forces.<sup>17</sup> In fact, our data shows that the pull off forces and  $F_{F0}/\mu$  have similar values and support the idea that both quantities reflect the contribution of adhesion to normal forces between the tip and specimen. The additive nature of the applied and adhesive forces is in good agreement with various models for elastic contacts that include adhesion.<sup>14,31</sup>

Average friction coefficients  $\bar{\mu}$  for each film were obtained from the best fit slopes to these data (**Figure (b)**). The friction coefficients  $\mu$  and  $\bar{\mu}$  obtained from the data in **Figure** fall between 0.1 and 0.4, and are comparable to AFM friction coefficients on other manganite thin films.<sup>6,10</sup> They are plotted against the thermal resistivity  $\kappa^{-1}$ , fluorine content  $x$ , and top layer thickness  $d$  of each film in **Figure 4(a)**. No systematic dependence of friction on the thermal resistivity can be seen, suggesting that friction is not controlled by the GHz to THz range phonons which control thermal conduction at room temperature.<sup>23</sup> Furthermore, these results indicate that the dissipation of heat by thermal conduction does not play a controlling role in friction.

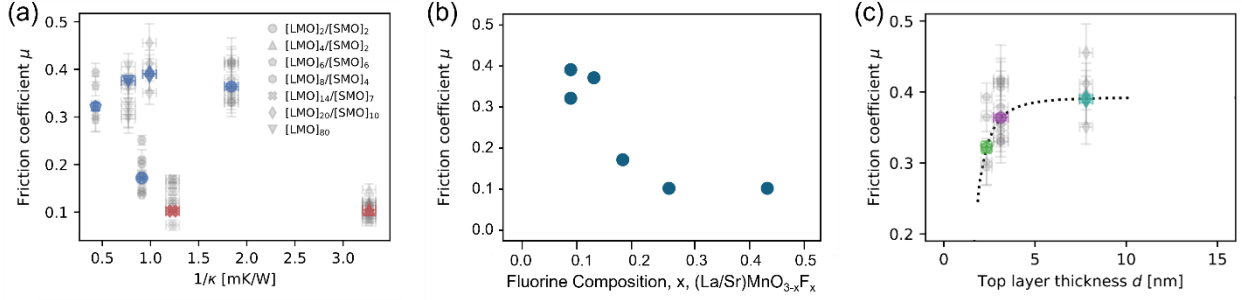


**Figure 4.** Friction coefficients of the superlattice films plotted against (a) thermal resistivity  $\kappa^{-1}$ , (b) fluorine content  $x$ , and (c) LaMnO<sub>3</sub> top layer thickness  $d$ . The friction coefficients  $\mu$  obtained from each individual Amonton measurement are shown as gray data points (from **Figure 3(a)**); the colored data points are the average values  $\bar{\mu}$  for each film (from **Figure 3(b)**). There is no apparent trend of friction coefficient with thermal resistivity (a), while the coefficients clearly decrease with increasing fluorine content (b). Among the specimens with low fluorine content, there is some indication that the friction coefficient decreases for thin LaMnO<sub>3</sub> top layer thicknesses (dashed line) (c).

In contrast, the friction coefficient is clearly reduced by the presence of fluorine (**Figure 4(b)**). The films with top layer thickness of  $m=2, 4$  and  $14$  exhibit high F concentrations and reduced friction coefficients compared to the other four films.

Within the set of three specimens containing the same fluorine content ([LMO]<sub>6</sub>/[SMO]<sub>6</sub>, [LMO]<sub>8</sub>/[SMO]<sub>4</sub>, and [LMO]<sub>20</sub>/[SMO]<sub>10</sub>), the thinnest top layer specimen ([LMO]<sub>6</sub>/[SMO]<sub>6</sub>) has a smaller average friction coefficient than the other 2 specimens (**Figure 4(c)**). Since the top layers of these three films have roughly the same compositions and similar surface roughness, the dissipative processes in the sliding contact interface are expected to be the same. Thus, any difference can be attributed to dissipation in the sub-surface material.

In contrast to the friction coefficient, the adhesive forces – either estimated from the pull-off forces or the values  $F_{F0}/\mu$  – vary strongly from position to position and show no systematic dependence on thermal conductivity, fluorine content, or layer thickness.

#### 4. Discussion

Friction forces were measured using lateral force microscopy on six manganite superlattice films with individual layer thicknesses ranging from 0.8 to 8 nm. The surface topography and frictional behavior remained unchanged during measurements, confirming that the tip-sample contact is

elastic within experimental resolution and that wear does not contribute significantly to the measured forces. Adhesion forces were found to vary with position—evident from the vertical shifts in the Amontons plots shown in **Figure 2(a)**—but were largely unaffected by fluorine doping or superlattice structure. In contrast, the friction coefficient for each specimen remained constant across its surface but varied systematically with both fluorine concentration and top-layer thickness. These trends and their implications are discussed to provide broader insights into mechanisms governing wear-free, sliding-contact frictional losses.

Adhesive forces, typically negligible in macroscale friction, become significant at the low normal loads applied in AFM studies. At the micro- and nanoscale, adhesion contributes to stiction, as it effectively adds an attractive normal force at the contact. The pull-off force measured from AFM force–displacement curves is widely accepted as a reliable measure of adhesion.<sup>17</sup> In our study, the ratio  $F_{F0}/\mu$  also serves as a useful proxy, where  $F_{F0}$  is the friction force at zero applied load and  $\mu$  is the friction coefficient. This ratio represents the tensile normal force required to exactly counteract adhesion and reduce the contact area to zero, assuming linear behavior.

Spatial variations in adhesion are attributed to local differences in surface chemistry and tip–sample contact geometry, which are sensitive to surface roughness. Variations in roughness and curvature may cause local fluctuations in water adsorption and solvent evaporation under ambient conditions. These, in turn, influence surface reactions such as carbon contamination or redox processes,<sup>32</sup> which directly affect adhesive forces. According to the Derjaguin–Muller–Toporov (DMT) model for a single-asperity, elastic–adhesive contact, the adhesive force is given by  $2\pi R\Delta\gamma$ , where  $R$  is the tip radius (assumed spherical) and  $\Delta\gamma$  is the change in surface energy per unit area upon contact.<sup>14</sup> The measured pull-off forces (3–75 nN, see SI-4.2) yield realistic values of  $\Delta\gamma$  between 0.05 and 1.20 J/m<sup>2</sup> for a nominal tip radius of  $R=10$  nm.<sup>31,33</sup>

Measured friction forces scale linearly with the total normal force, defined as the sum of the applied load  $F_N$  and the adhesive force. This supports the interpretation that adhesion contributes additively to the normal load.<sup>31,34</sup> Since friction is generally proportional to the true contact area between surfaces,<sup>35</sup> the observed linear dependence indicates that this area increases linearly with total normal force. In AFM contacts, the true contact area is determined by both surface roughness and the applied normal force. The linear scaling suggests a multi-asperity contact regime between the nominally spherical AFM tip and the nominally flat manganite film. In contrast, single-asperity

elastic contact—modeled by Hertzian theory—predicts a sublinear dependence of contact area on normal force, even when adhesion is included.<sup>29</sup> Several multi-asperity contact models, however, predict linear behavior,<sup>29</sup> and both regimes have been observed in AFM studies of hard materials. The specific regime depends on experimental factors such as tip radius, roughness, and applied load. Given the shallow indentation depths ( $< \text{a few } \text{\AA}$ ) and small contact diameters ( $\sim 3 \text{ nm}$ ) in our experiments, atomic-scale surface roughness on either the tip or film is sufficient to induce a multi-asperity contact and account for the observed linear friction–force relationship.

We observe a clear decrease in the friction coefficient with increasing fluorine doping. This is not surprising since fluorine doping is known to alter structural, electrical, and magnetic properties of manganites. In compounds such as  $\text{SrMnO}_{3-x}\text{F}_x$ , fluorine doping has been shown to induce ferromagnetism, trigger charge-ordered magnetic transitions through electron doping and local Mn-octahedral distortions,<sup>28</sup> and reduce electrical conductivity.<sup>36</sup> Similarly, fluorine incorporation leads to short-range magnetic ordering in  $\text{LaMnO}_{2.8}\text{F}_{0.2}$ <sup>37</sup> and induces ferroelectricity in  $\text{LaMnO}_2\text{F}$ .<sup>38</sup> Despite these substantial changes in bulk properties, fluorine doping does not affect adhesion forces, in agreement with XPS binding energy data indicating that fluorine is not a surface contaminant.

Among superlattice films with constant fluorine content, the sample with the thinnest  $\text{LaMnO}_3$  (LMO) top layer—2.3 nm—exhibits a 15% lower friction coefficient compared to samples with thicker top layers. This indicates that material properties up to  $\sim 5 \text{ nm}$  below the surface influence sliding friction. The data suggest that the underlying  $\text{SrMnO}_3$  (SMO) or the LMO/SMO interface reduces friction when located within  $\sim 5 \text{ nm}$  of the surface. It remains unclear whether the effect arises from intrinsic differences between LMO and SMO or from the presence of the interface itself. While  $\text{LaMnO}_3$  has a  $\sim 7\%$  lower elastic modulus than  $\text{SrMnO}_3$ ,<sup>39,40</sup> the resulting change in contact area—estimated using Hertzian contact mechanics—is less than 1% across the different top-layer thicknesses. Therefore, the observed reduction in friction for the  $[\text{LMO}]_6/[\text{SMO}]_6$  film is more likely due to a decrease in energy dissipation rather than contact area.

We propose that the dominant contribution to the measured friction arises from the generation and dissipation of mechanical excitations—such as stress fields, vibrations, and non-thermal phonons.<sup>6</sup> These excitations are primarily induced by Pauli repulsion forces and extend well beyond the immediate contact interface. For instance, recent theoretical studies modeling an oscillating AFM

tip have shown that evanescent waves and slowly moving stress fields dominate under AFM conditions and extend several nanometers below the surface. Similarly, simulations and analyses have demonstrated that the stress fields generated by an AFM tip in contact penetrate several nanometers into the sample.<sup>35</sup>

The idea that mechanical dissipation via internal friction contributes to sliding friction has been widely explored in the context of elastomers. Internal friction is commonly quantified by the inverse quality factor,  $Q^{-1}$ , and is often measured using mechanical spectroscopy. In elastomers—especially rubber—it is well-established that sliding friction scales with internal friction or elastic hysteresis losses.<sup>15,16</sup> Various theoretical models support this idea, proposing a linear relation of the form  $\mu_{IF}=C \cdot Q^{-1}$ , where  $\mu_{IF}$  is the friction coefficient due to internal friction, and  $C$  is a dimensionless proportionality constant.<sup>17,41,42</sup> This model explains energy dissipation from repeated loading and unloading of the material beneath the sliding asperity, and is consistent with observations in materials ranging from elastomers to metals.<sup>15</sup>

The proportionality constant  $C$  captures the mechanical and geometrical specifics of the contact, such as roughness, tip radius, and adhesion. For rubber sliding against rough surfaces,  $C$  is typically of order unity.<sup>17</sup> In the case of a single AFM tip with spherical radius  $R$  and circular contact radius  $a$ , the proportionality constant has been related to the local slope of the surface under the tip, estimated as  $a/R \approx 0.1$  based on Hertzian contact mechanics. However, this number should be considered a rough estimate, as smooth, continuous sliding at the nanoscale is likely an oversimplification.

In reality, several perturbations may affect the tip-sample interaction. Vibrations of the tip or sample, as well as dynamic processes at the contact interface, can result in partial or full unloading events. For example, if atomic-scale stick-slip occurs, the loading/unloading rate can increase substantially—up to  $v_s/\lambda$  where  $v_s$  is the tip sliding speed and  $\lambda$  is the atomic-scale slip distance. This is expected to lead to an increase in dissipated energy by a factor of  $2a/\lambda \approx 30$  compared to smooth sliding. Such dissipation via loading and unloading events turns up in microscopic models as evanescent waves, which decay exponentially into the material away from the surface,<sup>21</sup> where a quantitative comparison with  $Q$  factors is still missing. At typical AFM sliding speeds ( $\sim 1 \mu\text{m/s}$ ) and with atomic-scale roughness, the maximum frequency of such induced mechanical vibrations

is limited by the cantilever resonance ( $\sim 100$  kHz). Therefore, the tip-sample contact likely experiences mechanical excitations over a broad frequency range up to  $\sim 100$  kHz.

Although the value of  $C$  is challenging to determine, it should remain constant for a given contact configuration. From material property charts,  $Q^{-1}$  values range from  $\sim 1$  for elastomers to  $\sim 10^{-5}$  for materials like carbides and silicate glasses.<sup>43</sup> Sliding friction coefficients for dry contacts typically fall between  $10^{-3}$  and 1, implying a useful estimate of sliding friction within this modeling with practical values of  $C$  between 1 and 100, which are reasonable given the above discussion.

Mechanical spectroscopy studies of manganites have reported  $Q^{-1}$  values between  $10^{-4}$  and  $10^{-2}$ .<sup>44–46</sup> These spectra show a baseline loss from non-activated processes such as thermoelastic strain-temperature coupling, superimposed with broad peaks attributed to magnetic, structural, and charge-ordering transitions. These features arise from processes involving characteristic excitation and relaxation times. The range of reported  $Q^{-1}$  values is consistent with the friction coefficients measured in our experiments (0.1–0.4), supporting the idea that dissipation of mechanical excitations via internal friction is a viable explanation for the energy loss during AFM tip sliding.

Collectively, our findings paint a consistent picture of the tip-sample interaction during AFM friction measurements on manganite films. The data reveal an elastic, adhesive, multi-asperity contact where both contact area and friction force scale linearly with the total normal force. This is characteristic of non-wear friction regimes and suggests that our conclusions may be applicable to a broad range of materials beyond the manganites studied here. Notably, the independence of adhesion and friction coefficients implies distinct underlying mechanisms—adhesion being surface-controlled, while friction is governed by subsurface dissipation extending several nanometers below the surface.

Moreover, our findings demonstrate that friction can be tuned by adjusting the thickness of surface layers—a concept not limited to sliding contacts. A recent theoretical study of a non-contact AFM tip oscillating above a coated substrate found similar dependence of energy dissipation on top-layer thickness.<sup>21</sup> Under typical AFM conditions, the tip induces evanescent deformation waves that penetrate into the near-surface region to depths comparable to the vibration amplitude. The dominant energy loss arises from internal friction within this excited volume, with additional dissipation carried away by volume and surface waves.

#### 4. Conclusion

The AFM-based friction measurements of  $[\text{LaMnO}_3]_m/[\text{SrMnO}_3]_n$  superlattice films reveal a consistent picture of a multi-asperity elastic contact, where energy dissipation is captured by a robust and reproducible friction coefficient. This coefficient is relatively insensitive to surface conditions but strongly influenced by sub-surface material properties. We argue that the mechanisms governing this dissipation are closely related to those that control internal friction, offering a useful framework for understanding friction and selecting materials with tunable frictional behavior.

Our interpretation—that sub-surface energy dissipation via internal friction plays a dominant role in manganites—suggests new strategies for friction control, not only in complex oxides but also in other material classes and at larger length scales. Macroscale frictional contacts are typically composed of numerous nano- to microscale asperities, where similar sub-surface mechanisms may operate. In such systems, materials with higher internal friction offer greater potential for friction tuning through modifications of subsurface structure.

Notably, manganites exhibit higher internal friction than many other technologically relevant ceramics,<sup>43</sup> likely due to strong coupling between strain, spin, and charge degrees of freedom. This enhanced internal friction may explain the observed changes in sliding friction across phase transitions in several manganite systems.<sup>6,10</sup>

#### Supporting Information

Supporting Information is available from the Wiley Online Library or from the author.

#### Acknowledgements

This work was funded by the German Research Foundation (DFG) 217133147/SFB 1073, Project A01 and Project A02. The authors thank D.R. Baer, M.H. Engelhard from Pacific Northwest National Laboratory for discussion and help in interpreting the fluorine contamination observed in XPS measurements. We thank T. Brede for x-ray characterization of all films and SEM measurements of cantilevers. Additionally, we thank A. Wodtke and F. Güthoff from the Max Planck Institute for Multidisciplinary Sciences Göttingen for providing access and to maintain the Omicron VT-AFM system.



## References

- (1) Holmberg, K.; Erdemir, A. The Impact of Tribology on Energy Use and CO<sub>2</sub> Emission Globally and in Combustion Engine and Electric Cars. *Tribol. Int.* **2019**, *135*, 389–396. <https://doi.org/10.1016/j.triboint.2019.03.024>.
- (2) Binnig, G.; Quate, C. F.; Gerber, Ch. Atomic Force Microscope. *Phys. Rev. Lett.* **1986**, *56* (9), 930–933. <https://doi.org/10.1103/physrevlett.56.930>.
- (3) Bowden, F. The Area of Contact between Stationary and Moving Surfaces. *Proc. R. Soc. Lond. Ser. Math. Phys. Sci.* **1939**, *169* (938), 391–413. <https://doi.org/10.1098/rspa.1939.0005>.
- (4) Krylov, S. Yu.; Frenken, J. W. M. The Physics of Atomic-Scale Friction: Basic Considerations and Open Questions. *Phys. Status Solidi B* **2014**, *251* (4), 711–736. <https://doi.org/10.1002/pssb.201350154>.
- (5) Wang, W.; Dietzel, D.; Schirmeisen, A. Single-Asperity Sliding Friction across the Superconducting Phase Transition. *Sci. Adv.* **2020**, *6* (12), eaay0165. <https://doi.org/10.1126/sciadv.aay0165>.
- (6) Weber, N. A.; Schmidt, H.; Sievert, T.; Jooss, C.; Güthoff, F.; Moshneaga, V.; Samwer, K.; Krüger, M.; Volkert, C. A. Polaronic Contributions to Friction in a Manganite Thin Film. *Adv. Sci.* **2021**, *8* (8), 2003524. <https://doi.org/10.1002/advs.202003524>.
- (7) Altfeder, I.; Krim, J. Temperature Dependence of Nanoscale Friction for Fe on YBCO. *J. Appl. Phys.* **2012**, *111* (9). <https://doi.org/10.1063/1.4717983>.
- (8) Kisiel, M.; Gnecco, E.; Gysin, U.; Marot, L.; Rast, S.; Meyer, E. Suppression of Electronic Friction on Nb Films in the Superconducting State. *Nat. Mater.* **2011**, *10* (2), 119–122. <https://doi.org/10.1038/nmat2936>.
- (9) Kim, J. H.; Fu, D.; Kwon, S.; Liu, K.; Wu, J.; Park, J. Y. Crossing Thermal Lubricity and Electronic Effects in Friction: Vanadium Dioxide under the Metal–Insulator Transition. *Adv. Mater. Interfaces* **2016**, *3* (2), 1500388. <https://doi.org/10.1002/admi.201500388>.
- (10) Schmidt, H.; Krispeneit, J.-O.; Weber, N.; Samwer, K.; Volkert, C. A. Switching Friction at a Manganite Surface Using Electric Fields. *Phys. Rev. Mater.* **2020**, *4* (11), 113610. <https://doi.org/10.1103/PhysRevMaterials.4.113610>.
- (11) Qi, Y.; Park, J. Y.; Hendriksen, B. L. M.; Ogletree, D. F.; Salmeron, M. Electronic Contribution to Friction on GaAs: An Atomic Force Microscope Study. *Phys. Rev. B* **2008**, *77* (18), 184105. <https://doi.org/10.1103/PhysRevB.77.184105>.
- (12) Krim, J. Controlling Friction With External Electric or Magnetic Fields: 25 Examples. *Front. Mech. Eng.* **2019**, *5*. <https://doi.org/10.3389/fmech.2019.00022>.
- (13) Li, Y.; Wu, B.; Ouyang, W.; Liu, Z.; Wang, W. Experimental Decoding and Tuning Electronic Friction of Si Nanotip Sliding on Graphene. *Nano Lett.* **2024**, *24* (4), 1130–1136. <https://doi.org/10.1021/acs.nanolett.3c03642>.
- (14) Park, J. Y.; Salmeron, M. Fundamental Aspects of Energy Dissipation in Friction. *Chem. Rev.* **2014**, *114* (1), 677–711. <https://doi.org/10.1021/cr200431y>.
- (15) Tabor, D. The Mechanism of Rolling Friction II. The Elastic Range. *Proc. R. Soc. Lond. Ser. Math. Phys. Sci.* **1955**, *229* (1177), 198–220. <https://doi.org/10.1098/rspa.1955.0082>.
- (16) Grosch, K. The Relation between the Friction and Visco-Elastic Properties of Rubber. *Proc. R. Soc. Lond. Ser. Math. Phys. Sci.* **1963**, *274* (1356), 21–39. <https://doi.org/10.1098/rspa.1963.0112>.
- (17) Ciavarella, M.; Joe, J.; Papangelo, A.; Barber, J. R. The Role of Adhesion in Contact Mechanics. *J. R. Soc. Interface* **2019**, *16* (151), 20180738. <https://doi.org/10.1098/rsif.2018.0738>.

- (18) Zhang, D.; Li, Z.; Klausen, L. H.; Li, Q.; Dong, M. Friction Behaviors of Two-Dimensional Materials at the Nanoscale. *Mater. Today Phys.* **2022**, *27*, 100771. <https://doi.org/10.1016/j.mtphys.2022.100771>.
- (19) Filleter, T.; McChesney, J. L.; Bostwick, A.; Rotenberg, E.; Emtsev, K. V.; Seyller, Th.; Horn, K.; Bennewitz, R. Friction and Dissipation in Epitaxial Graphene Films. *Phys. Rev. Lett.* **2009**, *102* (8), 086102. <https://doi.org/10.1103/PhysRevLett.102.086102>.
- (20) Dong, Y. Effects of Substrate Roughness and Electron–Phonon Coupling on Thickness-Dependent Friction of Graphene. *J. Phys. Appl. Phys.* **2014**, *47* (5), 055305. <https://doi.org/10.1088/0022-3727/47/5/055305>.
- (21) Lee, M.; Weber, N.; Volkert, C. A.; Krüger, M. Friction on Layered Media: How Deep Do Phonons Reach? *Europhys. Lett.* **2023**, *142* (4), 46001. <https://doi.org/10.1209/0295-5075/acd140>.
- (22) Moshnyaga, V.; Khoroshun, I.; Sidorenko, A.; Petrenko, P.; Weidinger, A.; Zeitler, M.; Rauschenbach, B.; Tidecks, R.; Samwer, K. Preparation of Rare-Earth Manganite-Oxide Thin Films by Metalorganic Aerosol Deposition Technique. *Appl. Phys. Lett.* **1999**, *74* (19), 2842–2844. <https://doi.org/10.1063/1.124032>.
- (23) Meyer, D.; Metternich, D.; Henning, P.; Bange, J. P.; Gruhl, R.; Bruchmann-Bamberg, V.; Moshnyaga, V.; Ulrichs, H. Coherent Phonon Transport and Minimum of Thermal Conductivity in LaMnO<sub>3</sub>/SrMnO<sub>3</sub> Superlattices. arXiv August 12, 2021. <https://doi.org/10.48550/arXiv.2108.05860>.
- (24) Keunecke, M.; Lyzwa, F.; Schwarzbach, D.; Roddatis, V.; Gauquelin, N.; Müller-Caspary, K.; Verbeeck, J.; Callori, S. J.; Klose, F.; Jungbauer, M.; Moshnyaga, V. High-*T<sub>c</sub>* Interfacial Ferromagnetism in SrMnO<sub>3</sub>/LaMnO<sub>3</sub> Superlattices. *Adv. Funct. Mater.* **2020**, *30* (18). <https://doi.org/10.1002/adfm.201808270>.
- (25) Baer, D. R.; Engelhard, M. H.; Johnson, G. E.; Laskin, J.; Lai, J.; Mueller, K.; Munusamy, P.; Thevuthasan, S.; Wang, H.; Washton, N.; Elder, A.; Baisch, B. L.; Karakoti, A.; Kuchibhatla, S. V. N. T.; Moon, D. Surface Characterization of Nanomaterials and Nanoparticles: Important Needs and Challenging Opportunities. *J. Vac. Sci. Technol. Vac. Surf. Films* **2013**, *31* (5). <https://doi.org/10.1116/1.4818423>.
- (26) Vasequez, R. P. X-Ray Photoelectron Spectroscopy Study of Sr and Ba Compounds. *J. Electron Spectrosc. Relat. Phenom.* **1991**, *56* (3), 217–240. [https://doi.org/10.1016/0368-2048\(91\)85005-e](https://doi.org/10.1016/0368-2048(91)85005-e).
- (27) Briggs, D. Handbook of X-ray Photoelectron Spectroscopy C. D. Wanger, W. M. Riggs, L. E. Davis, J. F. Moulder and G. E. Muilenberg Perkin-Elmer Corp., Physical Electronics Division, Eden Prairie, Minnesota, USA, 1979. 190 Pp. \$195. *Surf. Interface Anal.* **1981**, *3* (4). <https://doi.org/10.1002/sia.740030412>.
- (28) Aich, P.; Meneghini, C.; Tortora, L.; Siruguri, V.; Kaushik, S. D.; Fu, D.; Ray, S. Fluorinated Hexagonal 4H SrMnO<sub>3</sub>: A Locally Disordered Manganite. *J. Mater. Chem. C* **2019**, *7* (12), 3560–3568. <https://doi.org/10.1039/c8tc04293d>.
- (29) *Fundamentals of Friction and Wear on the Nanoscale*, Third edition.; Gnecco, E., Meyer, E., Eds.; NanoScience and Technology; Springer International Publishing: Cham, 2024.
- (30) Cappella, B.; Dietler, G. Force-Distance Curves by Atomic Force Microscopy. *Surf. Sci. Rep.* **1999**, *34* (1–3), 1–104. [https://doi.org/10.1016/s0167-5729\(99\)00003-5](https://doi.org/10.1016/s0167-5729(99)00003-5).
- (31) The DMT Theory of Adhesion. In *Encyclopedia of Tribology*; Springer US: Boston, MA, 2013; pp 3560–3565. [https://doi.org/10.1007/978-0-387-92897-5\\_499](https://doi.org/10.1007/978-0-387-92897-5_499).

- (32) Rubasinghege, G.; Grassian, V. H. Role(s) of Adsorbed Water in the Surface Chemistry of Environmental Interfaces. *Chem. Commun.* **2013**, 49 (30), 3071. <https://doi.org/10.1039/c3cc38872g>.
- (33) Schwarz, U. D.; Zwörner, O.; Köster, P.; Wiesendanger, R. Quantitative Analysis of the Frictional Properties of Solid Materials at Low Loads. II. Mica and Germanium Sulfide. *Phys. Rev. B* **1997**, 56 (11), 6997–7000. <https://doi.org/10.1103/physrevb.56.6997>.
- (34) Derjaguin, B. V.; Muller, V. M.; Toporov, Yu. P. Effect of Contact Deformations on the Adhesion of Particles. *J. Colloid Interface Sci.* **1975**, 53 (2), 314–326. [https://doi.org/10.1016/0021-9797\(75\)90018-1](https://doi.org/10.1016/0021-9797(75)90018-1).
- (35) Fischer-Cripps. *Introduction to Contact Mechanics*.
- (36) Wang, J.; Shin, Y.; Gauquelin, N.; Yang, Y.; Lee, C.; Jannis, D.; Verbeeck, J.; Rondinelli, J. M.; May, S. J. Physical Properties of Epitaxial  $\text{SrMnO}_{2.5-\delta}\text{F}_\gamma$  Oxyfluoride Films. *J. Phys. Condens. Matter* **2019**, 31 (36), 365602. <https://doi.org/10.1088/1361-648x/ab2414>.
- (37) Mikhalev, K. N.; Lekomtsev, S. A.; Gerashchenko, A. P.; Yakubovskii, A. Yu.; Kaul', A. R. Short-Range Magnetic Order in  $\text{LaMn}(\text{O}_{1-x}\text{F}_x)_3$  from  $^{139}\text{La}$  and  $^{19}\text{F}$  NMR Data. *J. Exp. Theor. Phys. Lett.* **2003**, 77 (8), 401–404. <https://doi.org/10.1134/1.1587172>.
- (38) Xu, K.; Lu, X.-Z.; Xiang, H. Designing New Ferroelectrics with a General Strategy. *Npj Quantum Mater.* **2017**, 2 (1). <https://doi.org/10.1038/s41535-016-0001-8>.
- (39) None Available. Materials Data on  $\text{LaMnO}_3$  by Materials Project, 2020. <https://doi.org/10.17188/1193810>.
- (40) None Available. Materials Data on  $\text{SrMnO}_3$  by Materials Project, 2020. <https://doi.org/10.17188/1349743>.
- (41) Persson, B. N. J. On the Theory of Rubber Friction. *Surf. Sci.* **1998**, 401 (3), 445–454. [https://doi.org/10.1016/S0039-6028\(98\)00051-X](https://doi.org/10.1016/S0039-6028(98)00051-X).
- (42) Popov, V. L. *Contact Mechanics and Friction*; Springer Berlin Heidelberg: Berlin, Heidelberg, 2010. <https://doi.org/10.1007/978-3-642-10803-7>.
- (43) Ashby, M. F. *Materials Selection in Mechanical Design*, 4th ed.; Butterworth-Heinemann: Burlington, MA, 2011.
- (44) Zainullina, R. I.; Bebenin, N. G.; Burkhanov, A. M.; Ustinov, V. V.; Mukovskii, Ya. M. Longitudinal Sound Velocity and Internal Friction in Ferromagnetic  $\text{La}_{1-x}\text{Sr}_x\text{MnO}_3$  Single-Crystal Manganites. *Phys. Rev. B* **2002**, 66 (6), 064421. <https://doi.org/10.1103/PhysRevB.66.064421>.
- (45) Ma, Y. Q.; Song, W. H.; Zhao, B. C.; Zhang, R. L.; Yang, J.; Sheng, Z. G.; Lu, W. J.; Zheng, G. H.; Dai, J. M.; Du, J. J.; Sun, Y. P. Internal Friction Study on the Phase Separation Behaviour in  $\text{La}_{0.8}\text{Ca}_{0.2}\text{MnO}_3$ . *J. Phys. Condens. Matter* **2004**, 16 (41), 7447–7454. <https://doi.org/10.1088/0953-8984/16/41/024>.
- (46) Ma, Y. Q.; Song, W. H.; Zhang, R. L.; Dai, J. M.; Yang, J.; Du, J. J.; Sun, Y. P.; Bi, C. Z.; Ge, Y. J.; Qiu, X. G. Internal Friction Evidence of the Intrinsic Inhomogeneity in  $\text{La}_{0.67}\text{Ca}_{0.33}\text{MnO}_3$  at Low Temperatures. *Phys. Rev. B* **2004**, 69 (13), 134404. <https://doi.org/10.1103/PhysRevB.69.134404>.